Evolution of Low Earth Orbit Satellite Distributions

George Chiriac, Ionel Chiosa and Madalina Fron

Abstract

With a continuously growing number of satellites in the Low Earth Orbit region, the risk of overpopulation appears. In order to analyze this risk, as well as the time frame in which it is significant, we coded a program that extracts and processes data from a database of all satellites currently in orbit. We first used it to graph the current distributions of satellite orbits, in order for us to have a visual understanding of the population we are working with. We then developed equations that helped us find the evolution of these distributions due to atmospheric drag. In the first half of the paper we study only one orbital parameter at a time. In the second half, we employ statistical methods to study three orbital parameters simultaneously, creating spatial probability maps for one satellite and for several satellites, respectively. We reach the conclusion that, disregarding collisions between satellites, the risk of overpopulation naturally reduces in the time scale of 500 years, as atmospheric friction clears the satellite-dense region around the Sunsynchronous orbit.

1 Introduction

Beginning from the middle of the previous century, we have seen a continuous increase in the number of satellites in orbit around Earth. A high rate of satellite launches, along with an exponentially increasing rate of collisions, each producing additional debris fragments, leads to a rising risk of overpopulating our space environment. This "collisional cascading", studied by Kessler in his famous 1978 paper, may render space missions and satellite operation impossible for future generations. The effect is prominent in the Low Earth Orbit region, currently the most satellite-dense.

Our aim in this paper is to study atmospheric drag, a mechanism that works against collisional cascading by dragging satellites and debris into the atmosphere. In particular, we will find out the time necessary for atmospheric drag to clear the lower orbital environment. For this, we will study the evolution of the satellite population as a whole instead of restraining ourselves to a single object. Using the database provided by Space-Track.Org, we will analyze the distribution of satellite orbits with respect to their semimajor axis, eccentricity, and inclination, respectively. Exploiting the link between the semimajor axis and energy, we will create a simple but precise friction model that predicts the evolution of the semimajor axis distribution. Then, we will attempt to graph the spatial satellite density accounting for all three orbital parameters simultaneously, by switching from discrete positions of satellite orbits to probability densities.

The difficulties we have to overcome in analyzing the motion of a satellite are the intrinsic complexity of modeling perturbative interactions and the unpredictable rates at which satellites collide and are launched into orbit. Although most of these effects are important in particularly long time frames, we found a set of assumptions that can simplify our calculations drastically without creating significant errors:

- Perturbations to the elliptical orbit can be neglected in the time frame of a period
- There are no future satellite launches

- There are no collisions between satellites
- The initial coordinates of the satellite on its orbit are unknown and perigee precession leads to an arbitrary argument of periapsis
- One of the long term effects of the perturbations responsible for nodal precession is a completely arbitrary longitude

The first three assumptions are necessary for solving the evolution of orbital parameters. We will see how this is possible in the following sections.

2 Visualisation of the current satellite distributions

The database provided by Space-Track.Org in .xml format stores the orbit parameters of over 19000 satellites currently in orbit around Earth. We have coded a Javascript program that scans and parses the .xml document containing the database. Using it, we can construct various distribution functions of the satellites with regards to their orbit paramaters. The parameters of interest are the elliptical orbit's semimajor axis (hereafter noted as "a"), eccentricity (hereafter noted as "e") and inclination of the orbital plane (hereafter noted as "i").

2.1 Semimajor axis, eccentricity, and inclination distributions

To construct this distribution, we have split the domain of the semimajor axis (6500km-250000km) into intervals of 100km and found the number of satellites in each interval (a "satellite density"). Then, we have imported the data into a Microsoft Excel document to plot the obtained satellite density as a function of the semimajor axis. The resulting graph is shown below.

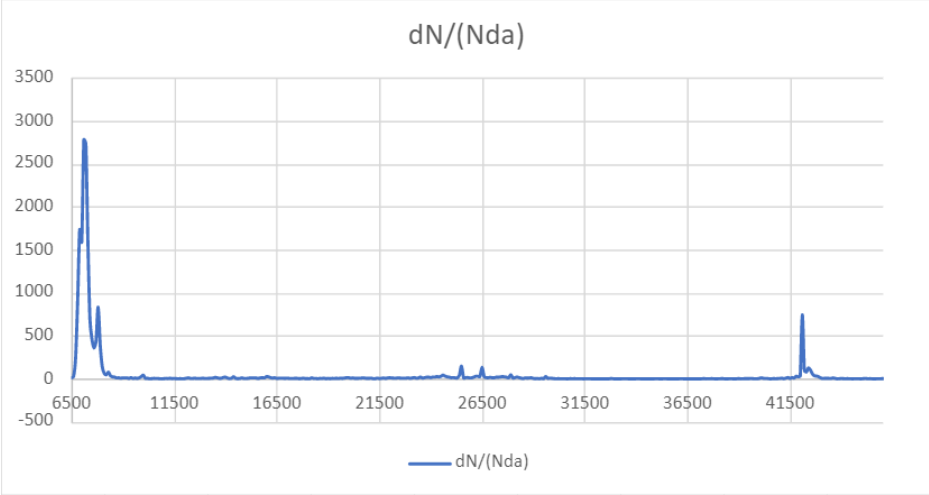

Figure 1: Horizontal axis: a. Vertical axis: Number of satellites between a and a+100km. We observe peaks around a=7200km, the Sunsynchronous orbit height, and around a=42000km, the Geosynchronous orbit height. These are the orbits of interest for commercial satellite use, therefore the densities of satellites in those regions are high.

In a similar procedure, we split the eccentricity domain (0-1) into intervals of 0.005 and obtained the satellite density as a function of eccentricity. This will be used later to calculate the average eccentricity. The resulting graph is shown below.

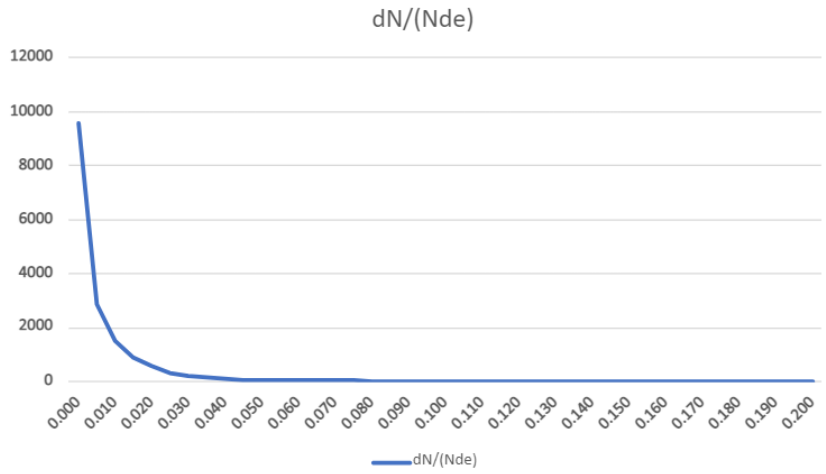

Figure 2: Horizontal axis: e. Vertical axis: Number of satellites with eccentricity between e and e+0.005. It is clear from the graph that most satellites have quasicircular orbits.

Similarly, we split the inclination domain (0-90) into intervals of 0.5. We obtained the following graph.

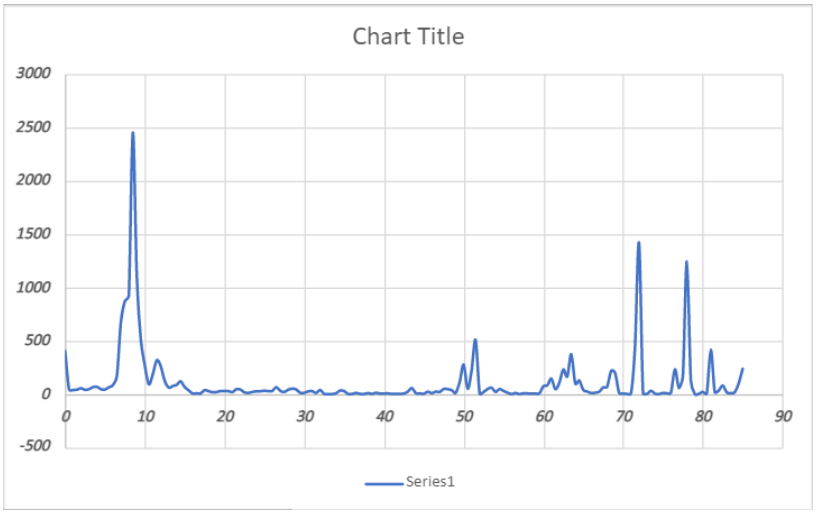

Figure 3: Horizontal axis: i. Vertical axis: Number of satellites with inclination between i and i+0.5.

3 Prediction and visualization of the evolution of current satellite orbits

Factors that alter the current distributions of satellites include collisions, radiation pressure and atmospheric drag. It has been shown (Kessler, 1978) that the only relevant altering mechanisms in medium timescales (hundreds of years) are collisions and atmospheric drag. The current collision rate of less than 1 per year does not significantly affect the satellite distributions. Therefore, in the following section, we will study only the evolution due to atmospheric drag. Atmospheric drag forces reduce an orbit's semimajor axis and its eccentricity. The speed at which this process works is proportional to the atmospheric mass density at the given altitude and the area to mass ratio of that object [Martin, 1967].

3.1 A note on atmospheric density

Recent atmospheric models have shown the atmospheric density to be negligible at altitudes over 1200km. Furthermore, drag forces become exceedingly strong at altitudes lower than 100km, and orbits in that region decay exponentially fast. Our domain of interest, then, lies between altitudes of 100km and 1200km. This corresponds to a semimajor axis range of around 6500km to 7700km. In this domain, the atmospheric density experiences high variations due to periodic solar activity and complex geomagnetic activity, photodissociation and diffusion phenomena (Kh.I. Khalil and S.W. Samwel, 2016). There are many atmosphere models (Jacchia, US Standard, MSIS), each predicting different time-dependent mass density profiles.

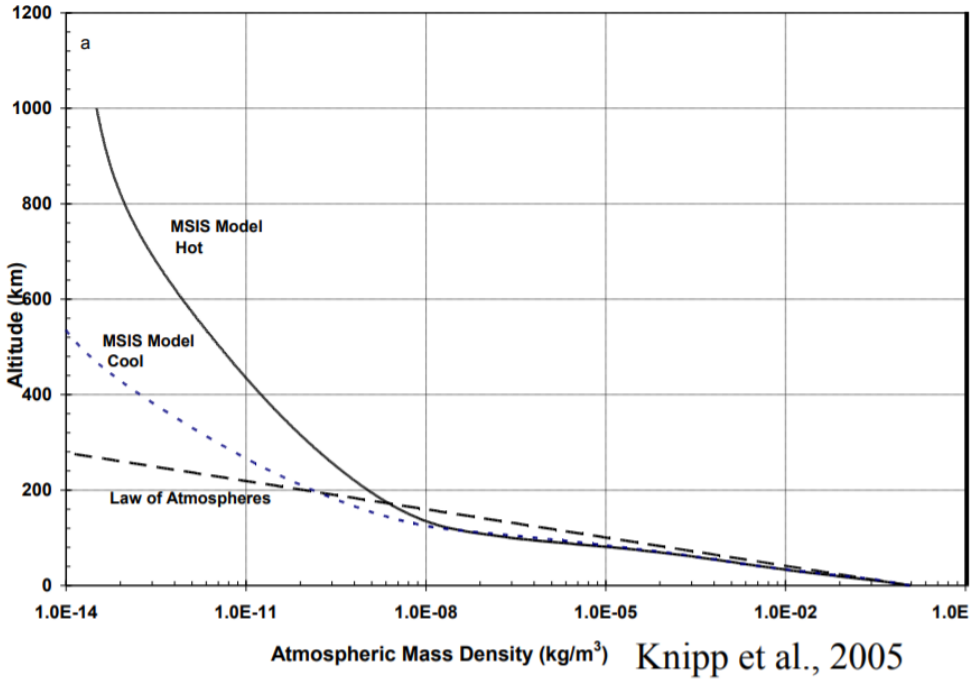

Figure 3

In this paper, we settled on a constant atmospheric density of $\rho = 1.2 * 10^{-14} \frac{kg}{m^3}$. This was obtained taking an average over different data sets predicted by the mentioned atmospheric models. This assumption does not affect the order of magnitude of our results and it gives us the possibility of treating the subject in the limits of high-school level physics. Furthermore, this leads to orbital decay periods in the studied range comparable to the ones calculated by Kessler (1978) and Brooks et al. (1975).

3.2 Analitical solution for the variation of the semimajor axis

In this section we will find how a varies for a single satellite. Our main assumption is that the orbit is quasicircular. To verify this assumption, we calculate the average eccentricity of all satellites in the database that fit into our studied range of altitudes. It turns out it is less than 0.01. Furthermore, if calculations for the variation of a are carried out accounting for eccentricity, the first term of the Taylor Expansion in e vanishes. Therefore, the error associated with neglecting e is of the order of 1%. We will use the known formula for dynamic friction,

$$\overrightarrow{F_f} = -\frac{1}{2} C_D A \rho v \overrightarrow{v}$$

E - total energy
A - cross-section of the satellite
C_D - friction coefficient (Assumed 2.2, the value for spherical satellites)
m - satellite mass
M- Earth's mass

The total energy in orbit:

$$E = -\frac{GMm}{2a}$$

$$\frac{dE}{dt} = \frac{GMm}{2a^2} \frac{da}{dt} \tag{1}$$

The energy change is equal to the work of friction:

$$\frac{dE}{dt} = \overrightarrow{F_f} \overrightarrow{v} = -\frac{1}{2} C_D A \rho v^3 \tag{2}$$

Assuming quasicircular orbits, we only centripetal acceleration exists:

$$m\frac{v^2}{a} = \frac{GMm}{a^2} \Rightarrow v = \sqrt{\frac{GM}{a}} \tag{3}$$

$$(1), (2), (3) \Rightarrow \frac{GMm}{2a^2} \frac{da}{dt} = -\frac{1}{2} C_D A \rho (\frac{GM}{a})^{\frac{3}{2}}$$

Integrating from present time to a future time, the semimajor axis decreases:

$$\int_{a_0}^{a} \frac{da}{\sqrt{a}} = -\rho C_D \sqrt{GM} \frac{A}{m} \int_0^t dt$$

Rearranging, we obtain the expression for the semimajor axis:

$$a = (\sqrt{a_0} - \frac{A}{m}\frac{\rho C_D \sqrt{GM}}{2}t)^2$$

$$Let \quad \gamma = \frac{A}{m}\rho C_D \frac{\sqrt{GM}}{2}$$

3.3 Calculation of the γ coefficient

In order to calculate γ for different satellites, we have to know the value of $\frac{A}{m}$. The Space-Track.Org database we use classifies satellites into three groups:

- Small A ($< 0.1\ m^2$)
- Medium A ($0.1\ m^2 <$ A $< 1\ m^2$)
- Large A (A $> 1\ m^2$)

We can use the satellite cross section distribution available in Kessler's paper, along with his empiric formula for the mass of a satellite as a function of its cross section ($m = 62A^{1,13}$), to calculate mean values of $\frac{A}{m}$ for each of the three satellite groups.

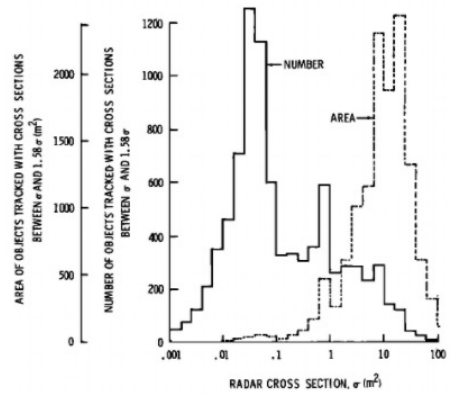

Figure 4: Cross Section distribution for a sample of 3000 satellites

We obtain:

- Small A: $(\frac{A}{m})_{avg} = 0.027\frac{m^2}{kg} \Rightarrow \gamma_{small} = 7.1 * 10^{-3}\frac{km^{\frac{1}{2}}}{yr}$
- Medium A: $(\frac{A}{m})_{avg} = 0.019\frac{m^2}{kg} \Rightarrow \gamma_{medium} = 5.0 * 10^{-3}\frac{km^{\frac{1}{2}}}{yr}$

- Large A: $(\frac{A}{m})_{avg} = 0.014 \frac{m^2}{kg} \Rightarrow \gamma_{large} = 3.7 * 10^{-3} \frac{km^{\frac{1}{2}}}{yr}$

3.4 Evolution of the semimajor axis distribution

To plot the semimajor axis distribution at a given, future time, we have compiled another Javascript program which identifies the A value group of each indexed satellite. Then, we use the equation derived in section 2.2 to find the value of the semimajor axis of each satellite at the given time. We proceed the same as described in section 1.1. Below are the graphs for the satellite distributions after 0, 100, 200, 300, 400 and 500 years from now, respectively.

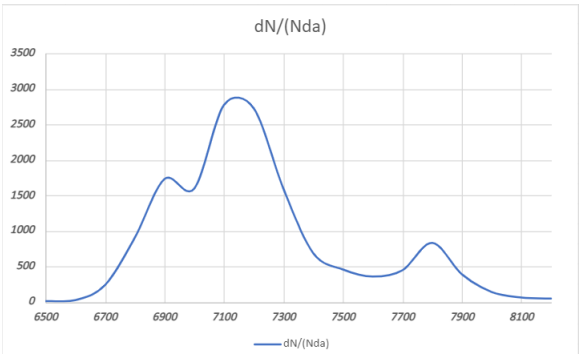

Figure 5: Present day

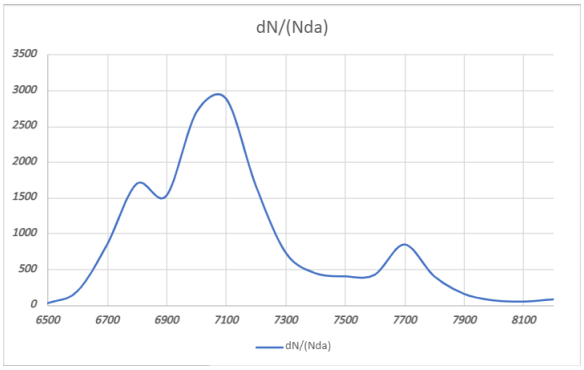

Figure 6: After 100 years

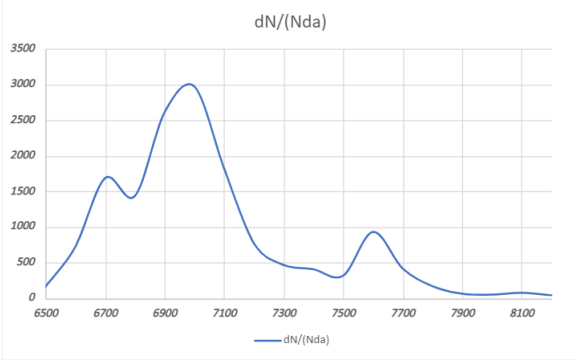

Figure 7: After 200 years

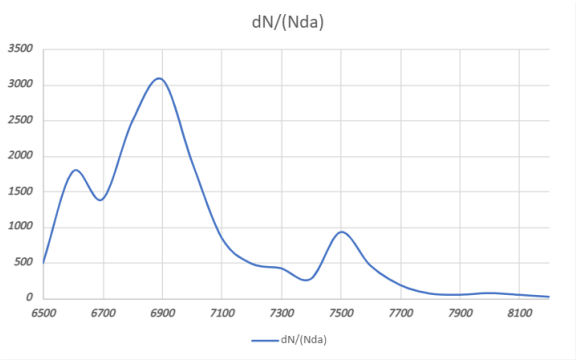

Figure 8: After 300 years

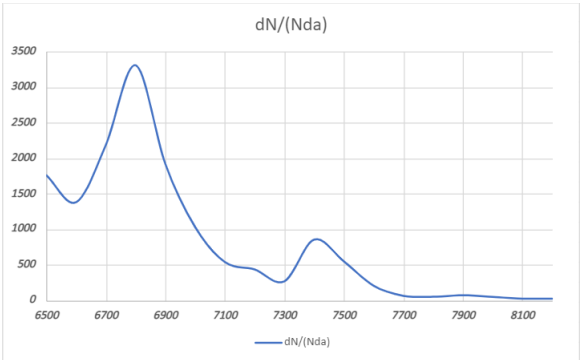

Figure 9: After 400 years

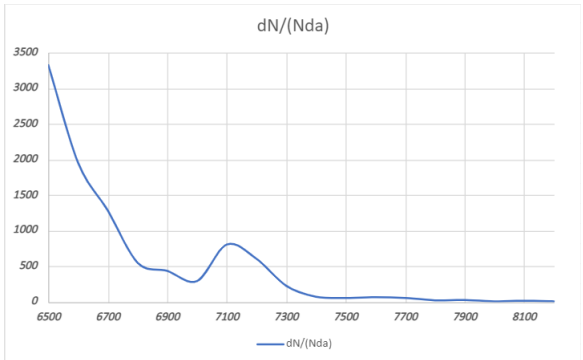

Figure 10: After 500 years

We observe two main effects. The first is that the distribution shifts to the left. This is due to all the semimajor axes decreasing. Notice that this effect is exponential in nature: while figures 5 and 6 are fairly similar, we see major differences between figures 9 and 10 for the same timescale of 100 years. The second effect is the sharpening of the peaks. This happens because the larger semimajor axes decrease faster than the smaller ones.

We have studied the evolution of our Space-Track.Org data with respect to one parameter. Now, we will generalise our study to account for the eccentricity and inclination of the orbital plane.

4 Generalization for all orbit parameters

The fourth and fifth assumptions listed in the introduction provide the tools necessary for intuitive and immediate visualizations of the orbital states of a satellite. More precisely, instead of solving for the instantaneous orbit of a satellite, which is very difficult to do when working in the set of assumptions mentioned, we will plot the probability density of finding the satellite in a particular region of space.

Firstly, we will ignore the effects of nodal precession and focus exclusively on the effects of the second assumption.

4.1 Planar probability map of one satellite

Let's consider an orbit that is characterized by the parameters p and e as follows:

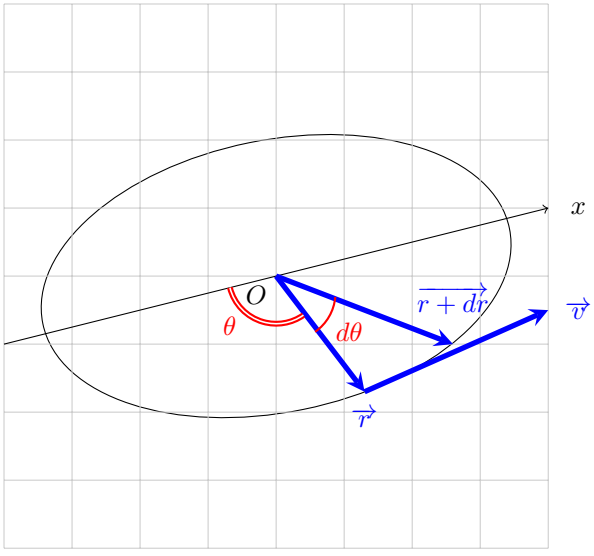

$$r(\theta) = \frac{p}{1 + e\cos\theta}$$

For the reasons mentioned above in the second assumption, the orientation of the perigee in the orbital plane

will be completely arbitrary. This will result in a distribution of probability independent of theta. In order to provide a visually pleasing illustration for this phenomenon, we plotted the trajectory of a satellite with a very eccentric orbit that has a significant deviation from its initial elliptical trajectory:

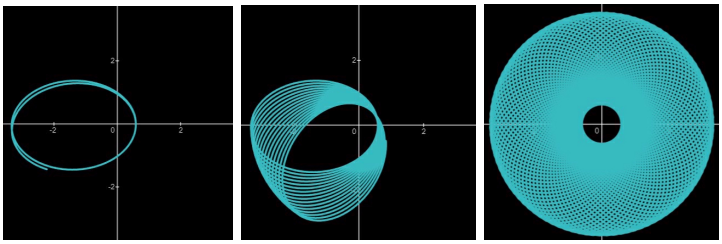

Figures 11,12,13

Because the probability of finding a satellite between r and r+dr is proportional to the time the satellite spent in that interval, we can write the following:

$$dP = f_s(r,\theta)2\pi r dr = \frac{dt}{T}$$

In order to find a relationship between the infinitesimal variations dr and dt, we have to analyse the trajecotry of the satellite more precisely.

$$f_s(r,\theta) = \frac{d^2P}{(rd\theta)dr}$$

From Kepler's Third Law:

$$\frac{T^2}{a^3} = \frac{4\pi^2}{GM} \qquad T = \sqrt{\frac{4\pi^2 a^3}{GM}}$$

$$dt = 2\frac{dr}{\dot{r}} \tag{4}$$

The orbit equation from above:

$$r(\theta) = \frac{p}{1 + e\cos\theta}$$

Taking the derivative of this expression with respect to θ:

$$r'(\theta) = \frac{pe\sin\theta}{(1+e\cos\theta)^2} = \frac{r^2 e\sin\theta}{p}$$

$$\dot{r} = \frac{dt}{dr} = \frac{dr}{d\theta}\frac{d\theta}{dt} = r'(\theta)\dot{\theta} = \frac{r^2\dot{\theta}e\sin\theta}{p} \tag{5}$$

The equation for angular momentum:

$$L = mrv_{\perp} = mr^2\dot{\theta} \Rightarrow r^2\dot{\theta} = \frac{L}{M} \tag{6}$$

$$(4), (5), (6) \Rightarrow dt = 2\frac{dr}{\frac{Le\sin\theta}{mp}}$$

Substituting the equation for dt in the infinitesimal probability, we obtain:

$$dP = \frac{dt}{T} = \frac{2mp}{Le\sin\theta}\frac{dr}{T}$$

$$\frac{dP}{2\pi r dr} = f_s(r,\theta) = \frac{1}{\pi}\frac{mp}{Le\sin(\theta)Tr} \tag{7}$$

Another expression for the angular momentum:

$$L = m\sqrt{GMp} \tag{8}$$

In the orbit equation, we solve for sin θ:

$$r = \frac{p}{1 + e\cos\theta}$$

$$\sin\theta = \sqrt{1 - \frac{1}{e^2}(\frac{p}{r} - 1)^2} \tag{9}$$

The known equation for the semi-latus rectum:

$$\sqrt{p} = \sqrt{\frac{b^2}{a}} \tag{10}$$

$$(7), (8), (9), (10) \Rightarrow f_s(r,\theta) = \frac{b}{2\pi^2 a^2}\frac{1}{\sqrt{(er)^2 - (p-r)^2}}$$

$$(er)^2 - (p-r)^2 = (er - p + r)(er + p - r) = (1+e)(r - \frac{p}{1+e})(1-e)(\frac{p}{1+e} - r)$$

The perigee and apogee distances, respectively:

$$r_m = \frac{p}{1+e} \qquad r_M = \frac{p}{1-e}$$

$$f_s(r,\theta) = \frac{b}{2\pi^2 a^2}\frac{1}{\sqrt{(1-e^2)(r - r_m)(r_M - r)}}$$

$$e^2 = 1 - \frac{b^2}{a^2}$$

Substituting, we finally obtain:

$$f_s(r,\theta) = \frac{1}{2\pi^2 a\sqrt{(r - r_m)(r_M - r)}}$$

If the value of the function is complex, the body never reaches that point because r is either bigger than r_M, or smaller than r_m. Plotting this function, we get the following figure for an orbit with convenient parameters:

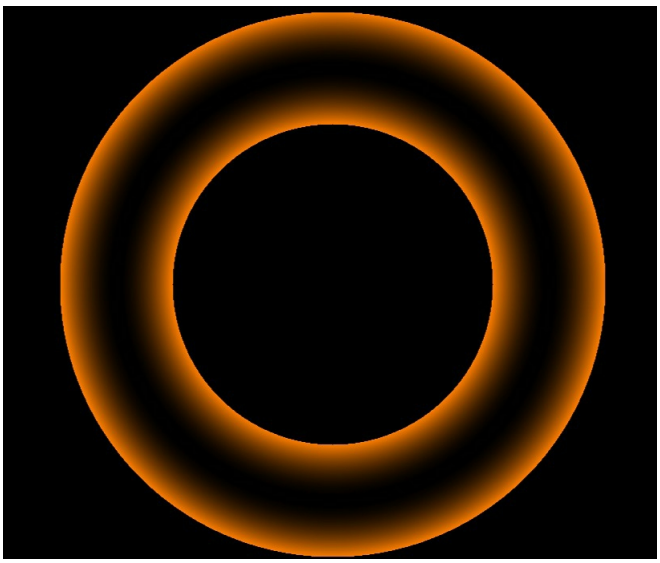

Figure 14: A high color intensity marks a high probability of finding the satellite in that region of space

4.2 Spatial probability map of one satellite

For the spatial density of probability, we have to take into consideration the implications of the fifth assumption, which will lead to the rotation of the plane density around Earth's axis.

In order to simplify our calculations, we introduced 2 new coordinate systems: the orthogonal (x, y, z) and the spherical (r, θ', ϕ).

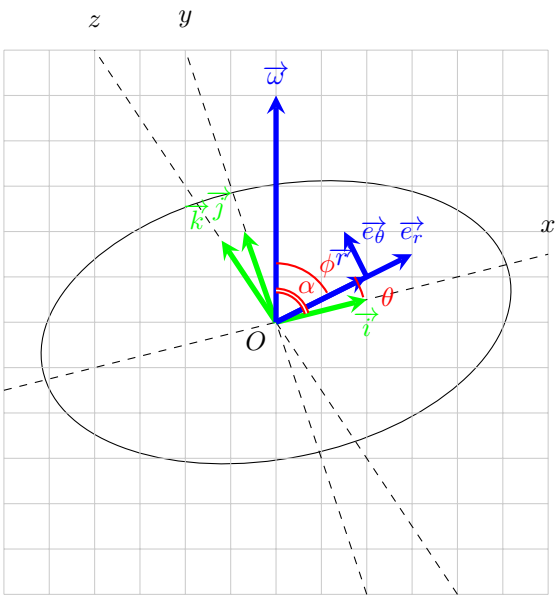

$\vec{\omega}$ - angular speed of the Earth
$\vec{i}, \vec{j}, \vec{k}$ - unit vectors such that $\vec{k}$ is perpendicular to the plane of the ellipse and $\vec{\omega} \cdot \vec{\alpha}$ is maximum. This means that $\vec{i}$ is coplanar with $\vec{k}$ and $\vec{\omega}$
ϕ - angle between $\vec{\omega}$ and $\vec{r}$, analogous to spherical coordinates
(r, θ, z) - cylindrical coordinate system such that r and θ are in the plane of the $f_r(r, \theta)$ distribution

$$\begin{aligned}
\vec{e_r} &= \vec{i}\cos\theta + \vec{j}\sin\theta \\
\vec{e_\theta} &= \vec{i}\sin\theta + \vec{j}\cos\theta \\
\vec{\omega} &= \omega\sin(\alpha)\vec{k} + \omega\cos(\alpha)\vec{i} \\
\cos\phi &= \vec{e_r}\frac{\vec{\omega}}{\omega} = \cos\omega\cos\alpha
\end{aligned} \tag{11}$$

Because the nodal precession rotates the initial plane probability density for an unspecified amount of time we can consider the final volumic distribution independent of the longitude θ'. For this reason, the probability of an element of area $rdrd\theta$ is redistributed on a ring of constant latitude and volume $rdrd\phi 2\pi r\sin\phi$. Thus, we can use the following:

$$f_V(r, \phi, \theta')2\pi r\sin(\phi)rdrd\phi = rdrd\omega f_r(r, \theta)$$

$$f_V(r,\phi,\theta') = \frac{f_r(r,\theta)}{2\pi r}\frac{d\theta}{\sin(\phi)d\phi}$$

$$(11) \Rightarrow \sin(\phi)d\phi = \sin\theta d\theta\cos\alpha$$

$$\frac{d\theta}{\sin(\phi)d\phi} = (\sin\theta\cos\alpha)^{-1}$$

$$\sin\theta = \sqrt{1-\frac{(\cos\phi)^2}{(\cos\alpha)^2}}$$

We obtain the equation for the spatial distribution due to nodal and perigee precession:

$$f_V(r,\phi,\theta') = \frac{f_r(r,\theta)}{2\pi r\sqrt{(\cos\alpha)^2-(\cos\phi)^2}}$$

Plotting the function in a plane that contains the vector $\overrightarrow{\omega}$ for an eccentricity of 0.16, we get this distribution:

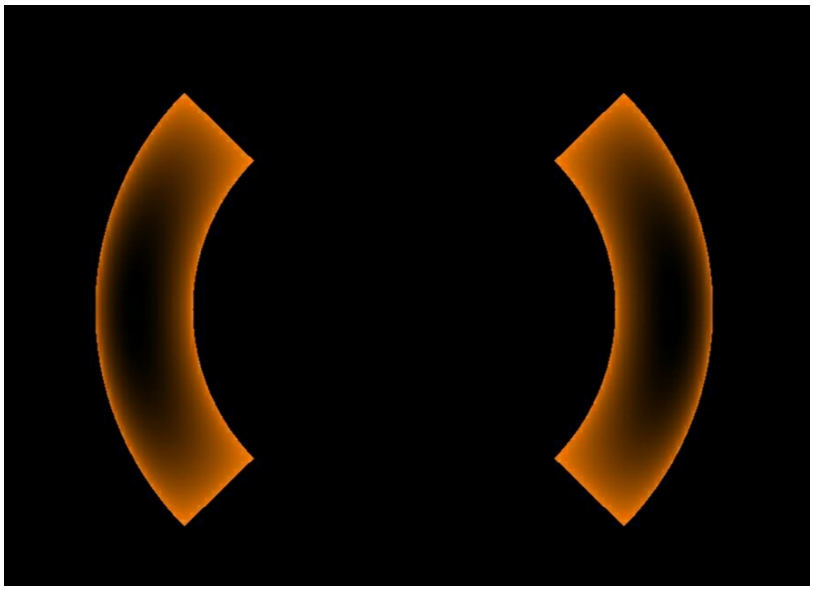

Figure 15: Section in the spatial probability map for an orbit with perigee and nodal precession

4.3 Spatial probability map of all satellites

Now, to find the total satellite density, we can use the method described above by overlapping the probability distribution for each satellite in the database. By doing so for different values of time, we can spot how satellite density varies in different spatial regions by simply comparing the diagrams.

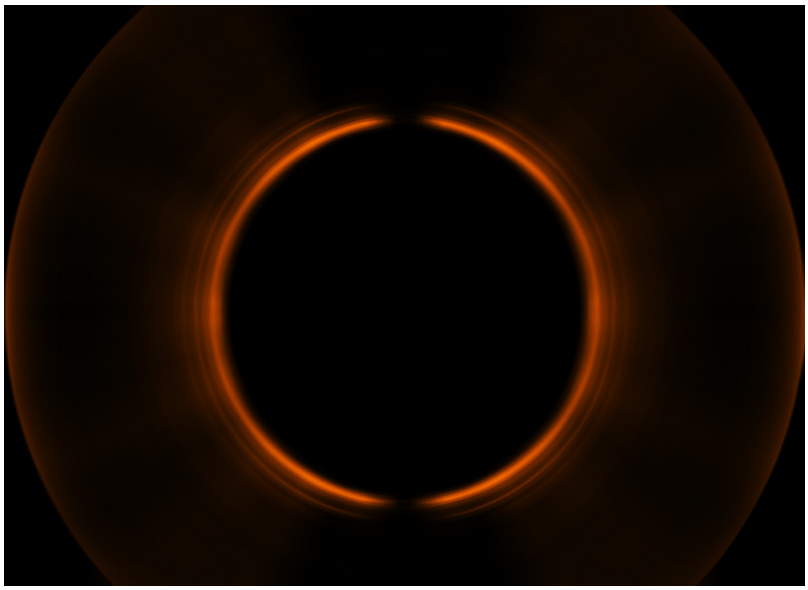

Figure 16: Section in the spatial probability map for all satellite orbits: present day

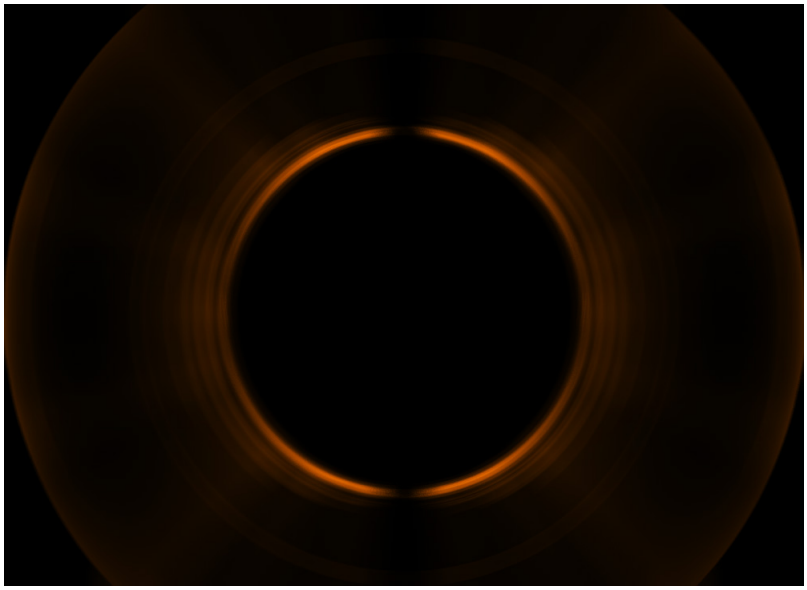

Figure 17: Section in the spatial probability map for all satellite orbits: after 500 years

5 Conclusion

One interesting feature of the distribution is the variation in the density of probability for polar and equatorial regions. As we can easily see in these two diagrams, the initial density of probability seems homogeneously distributed by latitude for the lowest earth orbit. However, the effect of atmospheric friction seems to affect low-latitude areas a lot more significantly than near-polar ones. This difference can be explained partially by the distribution of satellites by their orbital inclination, but a complete explanation requires a thorough

analysis of perturbative effects on satellite inclinations. Furthermore, we observe a slight thinning of the probability peak ring. This was expected from our previous analysis of the semimajor axis distribution: as satellites are dragged into the atmosphere, the low orbital environment is gradually cleared. With this in mind, collisional cascading may be less imminent than initially thought. Further study is required on the joint effect of all three orbit parameters on the variations of distributions in time, as well as the effect of a variable atmospheric density on the time dependence of the semimajor axis of a Low Earth Orbit satellite.

6 References

- https://www.space-track.org/
- https://agupubs.onlinelibrary.wiley.com/doi/abs/10.1029/JA083iA06p02637
- https://scialert.net/fulltext/?doi=srj.2016.1.9
- http://adsabs.harvard.edu/full/1960SCoA....5....9S
- https://apps.dtic.mil/dtic/tr/fulltext/u2/a392479.pdf